Experimental observation of quantum interferences in CO-H_2 rotational energy transfer at room temperature

Hamza Labiad,[1,*] Alexandre Faure,[2,†] and Ian R. Sims[1,3,‡]

[1] *Univ Rennes, CNRS, IPR (Institut de Physique de Rennes) - UMR 6251, F-35000 Rennes, France*
[2] *Université de Grenoble Alpes, CNRS, IPAG, F-38000 Grenoble, France*
[3] *Institut universitaire de France (IUF)*

Using time-resolved infrared–vacuum-ultraviolet double-resonance spectroscopy, experimental room temperature measurements of state-to-state rate coefficients for rotational energy transfer within the X $^1\Sigma^+(v=2)$ vibrational state of CO due to H_2 collisions have been compared to accurate 4-D close-coupling quantum calculations. Theoretically predicted quantum interferences in the CO-H_2 collisional system are experimentally observed at room temperature, and excellent agreement between theory and experiment is observed. These results provide a valuable benchmark for validating the anisotropic part of the potential energy surface, thereby supporting the theoretical modeling of CO emission in warm astrophysical environments such as photodissociation regions.

arXiv:2504.04403v3 [quant-ph] 9 Mar 2026

I. INTRODUCTION

Interacting systems inducing collisional energy transfer, are of great interest in many areas, ranging from astrochemistry [1, 2], atmospheric science [3], plasma and combustion [4–6], and gas lasers [7–10] to fundamental physical chemistry [11]. Measuring collision induced rotational energy transfer, RET, becomes crucial especially when chemical and physical processes of non-equilibrium gas phase environments are involved. Rate coefficients for RET are very sensitive to the potential energy surface (PES) of inelastic colliding systems making their measurement an ideal tool to accurately benchmark the quantum mechanical calculations with the objective to better understand the quantum phenomena that govern the elementary physico-chemical processes.

Measuring RET rate coefficients at very low temperatures ($T \lesssim 100$ K) has received a significant interest in the last decades because of the need for these rate coefficients in the fast-growing field of astrochemistry, and because of many interesting phenomena which are purely of a quantum nature, such as shape resonances. Experimental techniques have been significantly pushed forward for this purpose [12, 13], of course in addition to other cold chemistry purposes.

Somewhat less attention has been paid to the problem of measuring RET rate coefficients at relatively high temperatures despite its importance in completing the bigger picture of the theoretical benchmarking of both the attractive and repulsive parts of the PES. This is in part because techniques for accurately measuring RET rate coefficients have mainly been developed and adapted for low temperature studies.

On the other hand, even though diatom-diatom collisional systems may still appear relatively simple, they represent the most basic and important systems that must be well understood to gain confidence in studying more complex polyatomic collisional systems. In fact, very accurate full dimensional quantum close-coupling calculations on diatom-diatom systems were not possible until very recently. The quantum calculations of these systems become more complex if the number of channels is large (as is the case at higher temperatures for example), and even more complex if the collisional partner is an open-shell molecule. Recent examples include the CS + H_2 [14], SO + H_2 [15] and HCl + H_2 [16] systems.

The CO-H_2 system is an ideal diatom-diatom prototype for collisional systems involving nuclear-spin wave function of H_2, and a nearly homonuclear type molecule, CO. Interestingly, studying such a system can exhibit quantum effects at even relatively high temperatures in addition to low temperature quantum resonance effects, as observed in the CO-He [17], or in the NO-H_2 [18] systems. In fact, the quantum interference effect, predicted theoretically by the semiclassical model calculations of McCurdy and Miller [19], can be observed more easily at higher temperatures thanks to more transitions being available compared to lower temperatures. These interferences are characterized by strong propensity rules in final state populations. They are a consequence of the wave nature of matter and cannot be properly described by a quasi-classical trajectory (QCT) theory. Their origin in molecular scattering is conceptually similar to the classic Young's slit experiment where the two atomic centers of a diatomic molecule act as a 'molecular' double slit. In practice, the interference pattern depends on the relative magnitudes of the even and odd anisotropies of the PES. An illustrative example of the quantum nature of these propensities can be found in the work of Faure et al. [20] on the rotational excitation of HC_3N by H_2. These authors showed that the strong even Δj propensity observed in quantum close-coupling calculations was entirely absent in QCT results (see their Fig. 2). Recently, the mixed quantum/classical theory (MQCT) has also provided valuable time-dependent insight into this phenomenon [21].

Additionally, scaled AB-He collisional systems have long

* hamza.labiad@stfc.ac.uk
† alexandre.faure@univ-grenoble-alpes.fr
‡ ian.sims@univ-rennes.fr

been a proxy and less expensive alternative for AB-H_2 collisional systems. However, it has been shown that the two systems can differ significantly [22–24], and that separate quantum calculations and experimental studies for AB-H_2 are needed.

Succeeding in accurately measuring relatively high temperature RET rate coefficients and observing the quantum effects in the CO-H_2 system would then be a key tool for benchmarking the quantum calculations and would allow more confidence in the use of high temperature RET rate coefficients where CO in collision with H_2 is involved; for instance in probing photodissociation regions using high-j CO emission [25], as well as in nonlocal thermodynamic equilibrium models of the heating/cooling balance and physico-chemical processes in proto-planetary disks [26, 27].

II. THEORY

The same theoretical procedure as in [12] was employed. Rigid-rotor scattering calculations were performed with the MOLSCAT code [28] combined with the dedicated CO−H_2 four-dimensional (4D) $\langle V_{15}\rangle_{20}$ PES. This latter was obtained by averaging the high accuracy full six-dimensional V_{15} PES of Faure et al. [29] over the $(v = 2, j = 0)$ vibrational wavefunction of CO and the $(v_2 = 0, j_2 = 0)$ vibrational wavefunction of H_2. The resulting PES was then fitted with a spherical harmonic expansion, as described in [29] where full details can be found. In particular, a set of 60 basis functions was employed in the scattering calculations, including anisotropies up to l_1=7 and l_2=4, where the indices l_1 and l_2 refer to the angular dependence of the CO and H_2 orientation, respectively. We note that an even better 6D PES called V_{23} was published recently [30]. For scattering calculations, however, the differences with V_{15} are negligible [31]. It should also be noted that in our previous work, the rigid-rotor approach for CO in $v = 2$ was shown to be very accurate by comparison to full-dimensional scattering calculations (see Fig. 2 in [12]).

The rotational constants of CO and H_2 were fixed at the experimental values B_2(CO)=1.8875 cm^{-1} and B_0(H_2)=59.322 cm^{-1}. Convergence of the close-coupling calculations was carefully checked with respect to the basis set sizes and propagation parameters. Thus, the rotational basis set of CO included levels $j = 0 - 20$ and that of H_2 $j_2 = 0, 2$ for para-H_2 and $j_2 = 1, 3$ for ortho-H_2. The coupled differential equations were solved using the hybrid modified log-derivative Airy propagator from `RMIN`=3 to `RMAX`=200 a_0 (at low energy) with a step size always lower than 0.25 a_0. Cross sections were computed for collision energies in the range $3.9 - 2200$ cm^{-1} and state-to-state rate coefficients were deduced at 293 K by integrating the cross sections over a Maxwell-Boltzmann distribution of relative velocities. Since the measurements were performed with *normal*-H_2 (i.e., a para-H_2 to ortho-H_2 ratio of 1:3), the nuclear-spin weights of 1/4 and 3/4 were finally applied to the rate coefficients of para- and ortho-H_2, respectively.

III. EXPERIMENTAL METHOD

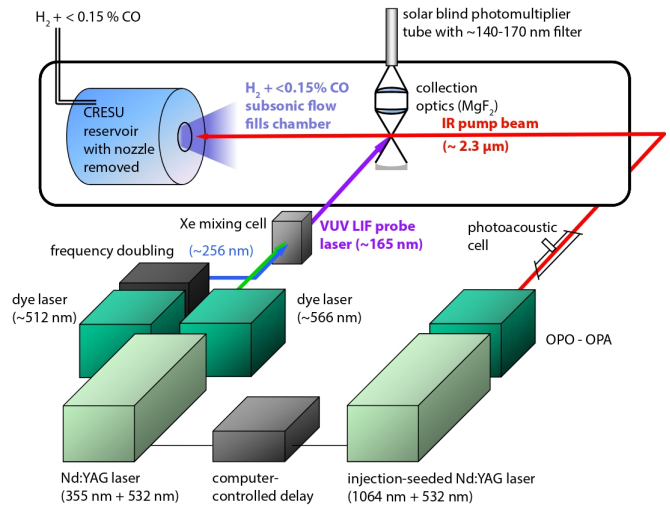

FIG. 1. Schematic diagram showing an overview of the experimental set up.

The measurements were made in a CRESU (French acronym for Reaction Kinetics in Uniform Supersonic Flow) apparatus combined with the infrared-vacuum ultraviolet, double resonance (IRVUVDR) technique. Although the CRESU apparatus was designed for low temperature studies, the room temperature measurements reported in this paper were not based on supersonic flows, instead, a subsonic laminar flow was generated by removing the nozzle assembly from the CRESU reservoir and introducing the gas in a manner to keep the reservoir and chamber pressures equal, avoiding any gas expansion (see Fig. 1).

CO and H_2 gases were introduced and mixed in the reservoir at very low CO concentrations ([CO]/[H_2] < 0.15%) in order to minimize CO self-collisions. In the fundamental electronic state, X $^1\Sigma^+$, quantum state-selected rovibrational states ($v = 2$, $j_i = 0$, 1 or 4) of CO molecules are prepared using tuneable IR laser pumping around 2350 nm. This radiation is generated by a combined optical parametric oscillator – optical parametric amplifier (OPO-OPA, LaserVision) pumped by an injection-seeded Nd:YAG laser (Continuum Surelite EX) operating at a repetition rate of 10 Hz with a pulse-duration of ∼5 ns, short enough to probe the fast kinetics of RET. The resulting infrared pulses had an energy of $\sim 5 - 10$ mJ. To ensure high data quality, it is crucial to have sufficiently populated initial rotational states, a condition which is not fulfilled in every IR pulse due to power and frequency fluctuations of the IR laser. A data discrimination process was applied using a photoacoustic reference cell filled with CO, through which

the IR laser was passed and fine-tuned to the transition line corresponding to the desired rotational state. Only data points with a photoacoustic signal intensity approximately 1.2 times the average photoacoustic signal were collected.

Under the influence of collisions with H_2, initially excited states of CO ($v = 2$, j_i) relax to final rovibrational states ($v = 2$, j_f). Vibrational relaxation is negligibly slow on the timescale of these experiments. The final states are probed by pulsed laser-induced fluorescence (LIF) via the $A\,^1\Pi(v = 0) \leftarrow X\,^1\Sigma^+(v = 2)$ vacuum ultraviolet (VUV) vibronic band of CO at ∼165 nm. This radiation was generated through 4-wave difference frequency mixing in Xe gas as described by Hilbig and Wallenstein [32]. In this method, two 256.01 nm photons excite the $5p^5\ 6p(5/2)_2 \leftarrow 5p^6\ ^1S_0$ transition of Xe, which is confirmed by sending the laser to a separate Xe filled reference cell in which a signal of (2+1) Resonance Enhanced Multi-photon Ionisation, REMPI, can be detected. A visible photon was tuned around 566 nm to stimulate the emission of a photon at the same wavelength and generating tuneable VUV at ∼165 nm. The 256.01 nm light was produced with a Sirah Lasertechnik Cobra-Stretch dye laser with Coumarin 503 dye (Exciton) pumped by a frequency tripled Continuum Precision II Nd:YAG laser (355 nm) operated at 10 Hz. The output of the dye laser (512.02 nm) was frequency doubled with a BBO crystal to produce ∼1 mJ of the desired 256.01 nm light. The frequency doubled output of the Nd:YAG laser (532 nm) also pumped a Laser Analytical Systems LDL 20505 dye laser operated with Rhodamine 6G dye (Exciton) dye to produce ∼8 mJ/pulse of ∼566 nm light. Both the visible and UV lasers were horizontally polarized, and were focused by an 18 cm (at 256 nm) focal length quartz lens through a fused silica window into a cell filled with 2.7 mbar of Xe. In addition, the visible light was prefocused through a 150 cm (at ∼566 nm) focal length lens. The VUV light produced was re-collimated by a 10.4 cm (at 166 nm) focal length MgF_2 lens (Crystran Ltd) into the CRESU chamber perpendicular to the horizontally polarized IR laser beam. In this configuration the double resonance signal is not sensitive to any polarization alignment effects. It is important to perfectly overlap the UV and visible laser pulses inside the Xe mixing cell both in space and time in order to produce the VUV radiation. Following the probe pulse, the resulting LIF was detected by a solar blind photomultiplier tube, (PMT, ET Enterprises 9403B) equipped with a bandpass interference filter (Acton Research) centered at 158.9 nm with a 23.4 nm bandwidth. The signal from the PMT was sent to a Stanford Research SR250 gated integrator with a 16 ns gate and sent to the computer to be recorded. Timing between the IR and the VUV pulses was controlled with two digital delay generators (Stanford Research SR535).

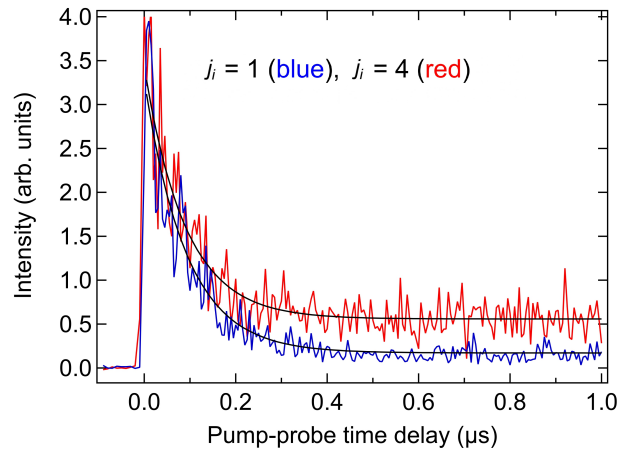

FIG. 2. Typical scaled LIF decays (blue and red) for $j_i = 1$ and $j_i = 4$, with $[H_2]$ densities of 1.6 x 10^{16} and 2.4 x 10^{16} molecule cm^{-3}, respectively, and their exponential fits (black) used to estimate total removal rate coefficients. The LIF signals are recorded by tuning the pulsed IR laser on the R(0) and R(3) line transitions for state-selective preparation of $j_i = 1$ and 4 respectively, tuning the pulsed VUV laser on the prepared initial state j_i using the Q(1) and R(4) line transitions for $j_i = 1$ and 4 respectively and monitoring in time the fluorescence signal using a solar blind PMT.

IV. EXPERIMENTAL PROCEDURE AND DATA ANALYSIS

Similarly to our previous work [12, 33], two types of experiments were performed: a so called *spectroscopic* experiment where state-to-state rate coefficients are measured using spectra recorded at different time delays, and a *kinetic* experiment in which the population decay of the initially pumped rovibrational state is monitored in time. Details of the experimental procedure and data analysis are present in previous papers [12, 33, 34], and only a short overview is given here.

In *kinetic* experiments, total removal rate coefficients are measured by initially preparing a pure single rotational state j_i in $v = 2$ using a pulsed tuneable IR laser, and a second pulsed tuneable VUV laser is used to monitor the LIF decay of the population measured in the line $Q(j_i)$ as a function of time. $Q(j_i)$ transition lines of the $A\,^1\Pi(v = 0) \leftarrow X\,^1\Sigma^+(v = 2)$ band of CO are chosen as they are well resolved and more intense compared to other branch lines. Fig. 2 illustrates typical time removal signals for $j_i = 1$ and 4. First order exponential decay rate coefficients k_{exp} are estimated using a Levenberg-Marquardt fitting algorithm. Reverse collisional processes are considered and assumed to arise from a Boltzmann equilibrium distribution of states in $v = 2$. Total removal coefficients are given by:

$$k_{tot} = \frac{k_{exp}\left(1 - f_{j_i}^{eq}\right)}{[H_2]} \tag{1}$$

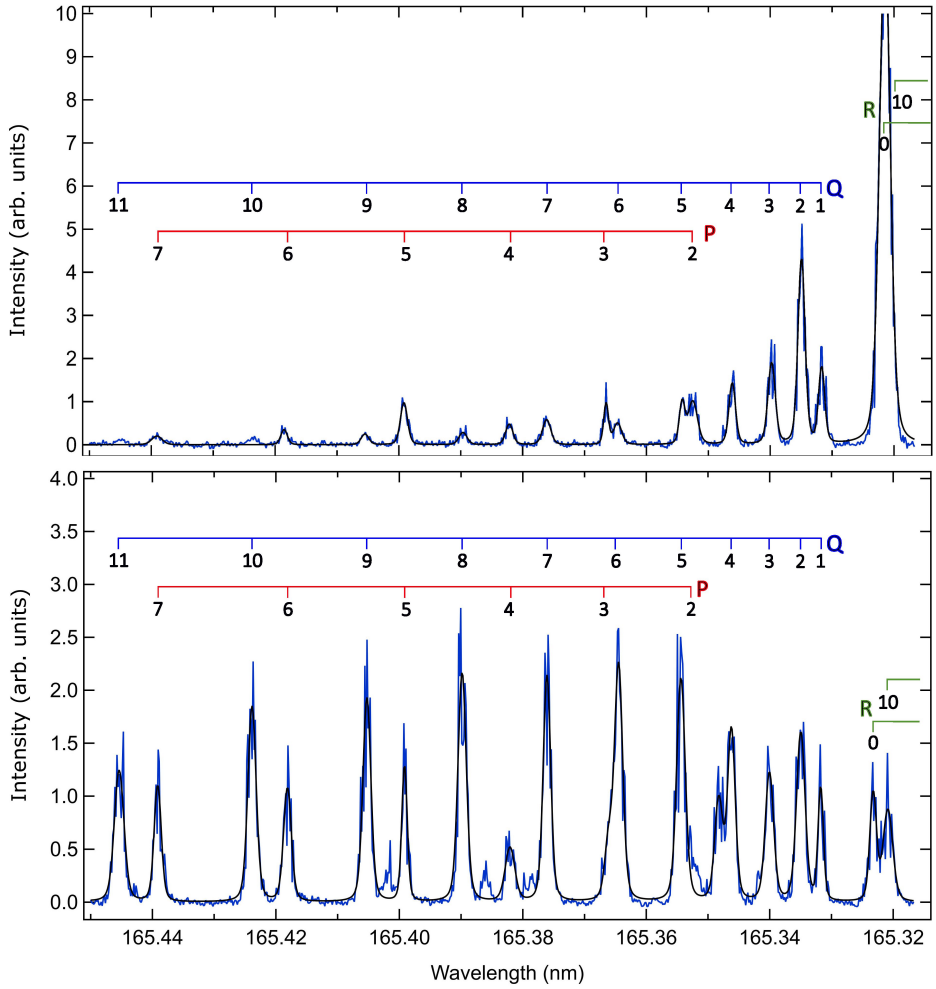

FIG. 3. Short- and long-time delay spectra for $j_i = 0$ at 293 K (blue) with multipeak Voigt fitting (black).

where $f^{eq}_{j_i}$ is the Boltzmann factor of j_i at rotational equilibrium divided by the partition function, and $[H_2]$ is the number density of H_2. The LIF signal decays exponentially to a non-zero value where the ratio of this value to the maximum initial intensity represents the Boltzmann factor, which can be used as an additional confirmation of the temperature of the gas, 293 K. In *spectroscopic* experiments, following the initially prepared state j_i, a pulsed tunable VUV laser is scanned over all the wavelength range of possibly measured final rotational states j_f ($j_f = 0 - 9$ or 10). Two spectra are recorded, one at very short time delay when only a small fraction of RET has occurred, typically at 15 to 30 ns after the IR pump, and another one at 2 - 3 μs when thermal rotational equilibrium has been reached but without significant vibrational relaxation. Voigt lineshapes are fitted to each peak in both spectra (see Fig. 3) in order to extract the line intensities which are then used to obtain state-to-state rate coefficients according to the formula:

$$k_{j_i \to j_f} = \left(\frac{I^{\delta t}_{j_f} f^{eq}_{j_f}}{I^{eq}_{j_f}} \right) \frac{1}{\delta t [H_2]} \tag{2}$$

where $I^{\delta t}_{j_f}$ is the line intensity corresponding to the final rotational state j_f at short time delay δt, $f^{eq}_{j_f}$ is the Boltzmann factor (fractional population at rotational equilibrium) for j_f and $I^{eq}_{j_f}$ is the line intensity for j_f at equilibrium. The validity and details of the derivation of equations (1) and (2) are discussed in previous work [34, 35].

V. RESULTS AND DISCUSSION

Table I and Fig. 4 show very good agreement between the experimental and theoretical state-to-state rate coefficients. The small differences outside of the experimental error bars are likely due to slightly underestimated systematic errors in the measurements.
We can make the following observations:

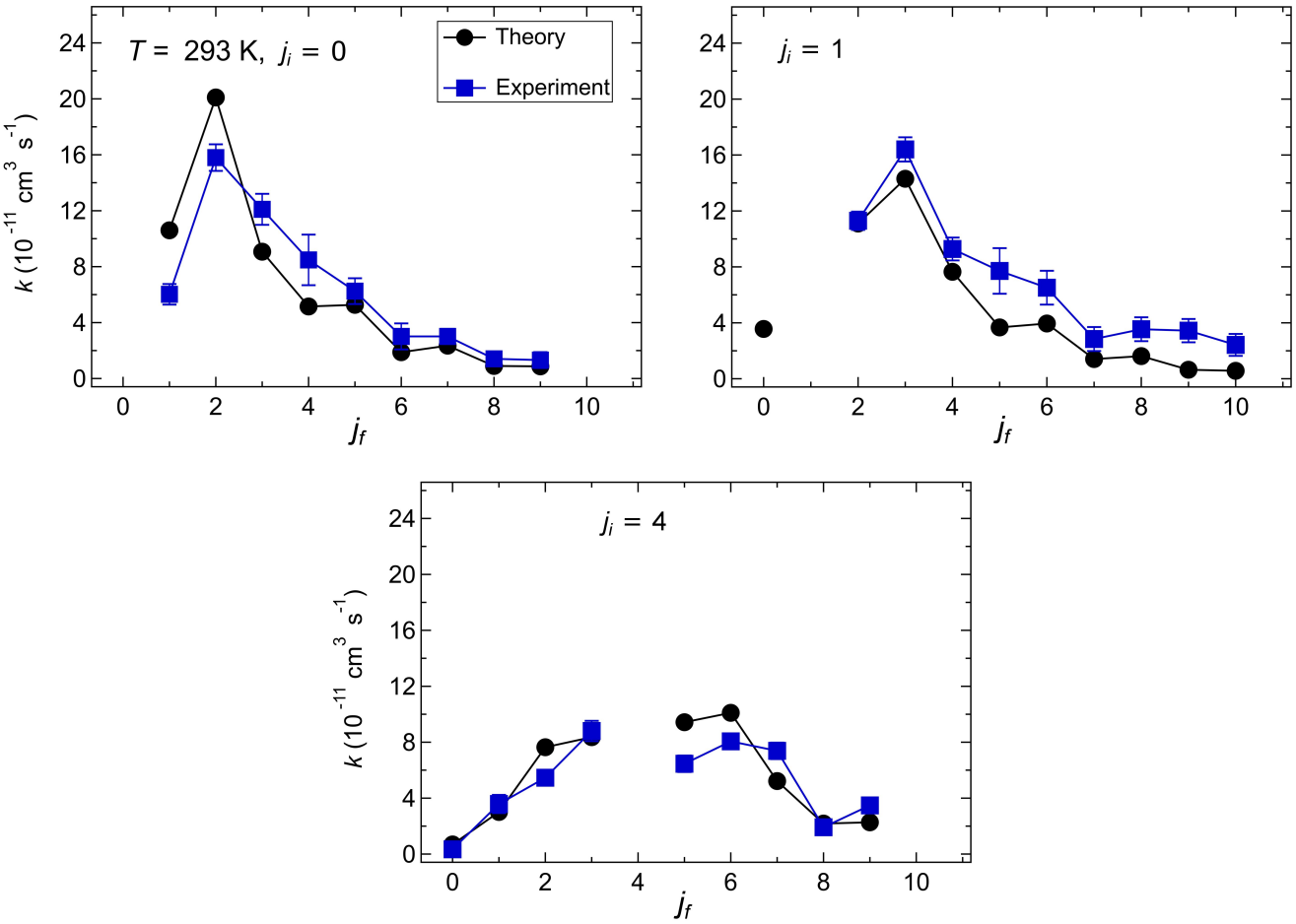

FIG. 4. Measured state-to-state rate coefficients (squares) and theoretical state-to-state rate coefficients (circles), calculated using the 4D $\langle V_{15}\rangle_{20}$ PES for $j_\mathrm{i} = 0, 1$ and $4 \rightarrow j_\mathrm{f}$ at 293 K. Error bars correspond to 2σ statistical errors.

(i) The rate coefficients decrease with increasing $|\Delta j|$;

(ii) Larger rate coefficients are, in general, observed at-room temperature compared to low temperatures [12]

(iii) Transitions with $\Delta j = +2$ are significantly favoured for low j_i (0 and 1);

(iv) An even propensity rule is observed for low Δj, switching to an odd propensity rule for large Δj;

(v) Different propensity rules and magnitudes are observed compared to the CO-He system.

These observations can be explained as follows.
(i) The observed decrease with increasing $|\Delta j|$ is due to the fact that high Δj transfers require a greater amount of collision energy according to the general energy gap law [36]. We can see though a relatively wide distribution of state-to-state rate coefficients as the CO rotational energy spacing is very small compared to the available collision energy at room temperature, thus favoring large energy transitions.
(ii) The generally larger rate coefficients observed at room temperature compared to low temperature values [12] can be explained by two effects causing the increase of RET rate coefficients where each one dominates over a different temperature range: the collisional energy and the long-range interaction. The latter dominates at low temperatures as the collisional energy drops below the 88.5 cm^{-1} well depth [29] i.e. in the resonance regime, and the former dominates at higher temperatures. This is illustrated in Fig. 5 where the theoretical and experimental rate coefficients for rotational excitation and de-excitation of CO ($j_i = 1$) are plotted as functions of temperature. The resonance regime is observed below $\sim$ 30 K for the $j_i = 1 \rightarrow 0$ exothermic transition while the energy criterion applies for all endothermic transitions. We also note that the even Δj propensity rule is observed above $\sim$ 30 K, due to the larger rotational threshold of the $j_i = 1 \rightarrow 3$ transition (28 K) compared to $j_i = 1 \rightarrow 2$ (11 K). The even Δj propensity rule is indeed observed at the cross section level down to the

	$j_{initial}$		
j_{final}	0	1	4
0	$j_{initial}$	-	0.34 ± 0.1 (0.7)
1	6.02 ± 0.7 (10.6)	$j_{initial}$	3.58 ± 0.6 (3.0)
2	15.8 ± 0.9 (20.1)	11.3 ± 0.7 (11.1)	5.46 ± 0.5 (7.6)
3	12.10 ± 1.1 (9.1)	16.4 ± 0.9 (14.3)	8.80 ± 0.7 (8.4)
4	8.48 ± 1.8 (5.2)	9.28 ± 0.8 (7.7)	$J_{initial}$
5	6.25 ± 0.9 (5.3)	7.71 ± 1.6 (3.7)	6.46 ± 0.6 (9.5)
6	3.01 ± 0.9 (1.9)	6.51 ± 1.2 (4.0)	8.06 ± 0.5 (10.1)
7	3.01 ± 0.5 (2.3)	2.84 ± 0.9 (1.4)	7.38 ± 0.6 (5.2)
8	1.41 ± 0.5 (0.9)	3.54 ± 0.9 (1.6)	1.92 ± 0.5 (2.2)
9	1.32 ± 0.6 (0.9)	3.44 ± 0.8 (0.7)	3.48 ± 0.7 (2.3)
10	-	2.42 ± 0.8 (0.6)	-
$\Sigma k_{st\to st}$	57.4 ± 2.9 (56.3)	63.5 ± 3.0 (45.1)	45.5 ± 1.6 (49.0)
k_{Total}	32.2 ± 1.7 (56.3)	42.2 ± 2.9 (45.1)	33.8 ± 4.0 (49.0)

TABLE I. Measured state-to-state rate coefficients and theoretical values (in parentheses) for RET in CO – H_2 collisions, calculated using the 4D $\langle V_{15}\rangle_{20}$ PES, for $j_i = 0, 1$, and $4 \to j_f$ at 293 K. Units are in 10^{-11} cm^3 s^{-1} and error limits correspond to 2σ statistical errors. The sum of the state-to-state rate coefficients, Σk, and the equivalent rate coefficients, k_{tot}, from kinetic experiments are also given.

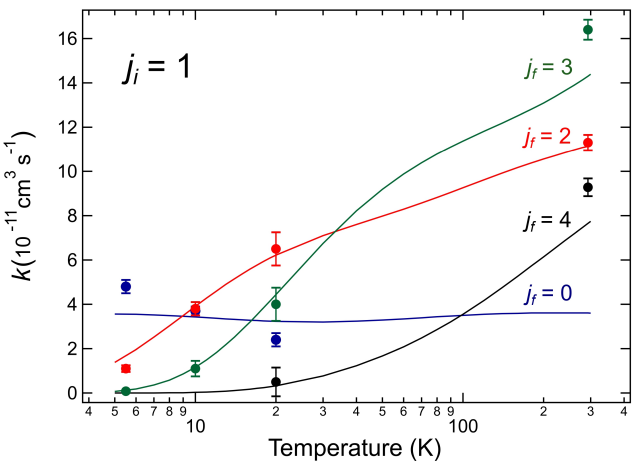

FIG. 5. Theoretical (solid lines) and experimental (circles) rate coefficients for the rotational (de)excitation of CO($j_i = 4 \to j_f = 0, 1, 2, 3$) by *normal*-$H_2$ as a function of kinetic temperature. Experimental data points between 5.5 K and 20 K are taken from [12].

excitation thresholds.

(iii) A clear even Δj propensity rule is observed for the CO-H_2 system. This is due to quantum interferences which were predicted and explained by McCurdy and Miller [19] for near homonuclear molecules. Only a few studies have reported experimental observations of even propensity rules [37–40]. To the best of our knowledge, the even propensity rule has never been experimentally observed for CO in collision with any atom or molecular species, except in our previous work at low temperatures where the $\Delta j = +2$ propensity rule was observed for $j_i = 0$ at 20 K [12].

(iv) In the case of CO in collisions with He, an interference structure was observed at low Δj in the experiment of [41]. However, no clear propensity for even or odd Δj was evidenced because their measurements were not sufficiently state-selected. In particular, the initial CO rotational distribution was not state-selective with about 70% of $j = 0$ and 30% of $j = 1$. In this study, we were able to measure pure state-to-state rate coefficients and to observe not only the even propensity for small Δj, but also the odd propensity for large Δj, as predicted theoretically by McCurdy and Miller [19]. As discussed by these authors, resolving this interference structure is a sensitive probe of the anisotropy of the PES because the even and odd propensities directly reflect the competition between terms with even and odd orders in the spherical harmonic expansion of the PES. A change of propensity was thus found for CO + p-H_2 by Mengel et al. [42] when using the first 'high-accuracy' PES for CO-H_2 [43]: low temperature rates for $\Delta j = -2$ were found to be smaller than those for $\Delta j = -1$, in contrast to previous studies based on older and less accurate PES. This result, which conflicts with the even propensity rule, was attributed by Mengel et al. to additional resonances in the $|\Delta j = 1|$ cross sections calculated with the new PES. An even more significant effect of the PES on the propensity rules was observed in CO + H and was ascribed to the long-range behavior of the PES [44–46]. It is however important to mention that subsequent refinements of the CO-H_2 or CO-H PESs have not changed the propensity rules significantly, while they have noticeably improved the rovibrational spectrum of the complex and the magnitudes of the rate coefficients. We also recall that in this study *normal*-H_2 was employed so that the magnitude of the rate coefficients is the weighted sum (1/4 and 3/4) of rate coefficients for CO in collision with p-H_2 and o-H_2. These, however, typically differ by less than 20%.

(v) Compared to the CO-He system [34], CO-H_2 exhibits higher rate coefficients and different propensity rule behavior. In particular, rate coefficients for $\Delta j = 2$ for CO-H_2 are four times larger than those of CO-He for $j_i = 0$ and 1, and double for $j_i = 4$. This provides clear experimental evidence to underline the now well established observation that AB-He data should not be used as a scaled surrogate for AB-H_2 systems.

Finally, we note that though the energy gap model does describe the overall dependence of the rate coefficients with Δj, it is clearly unable to reproduce the detailed behavior observed in this study owing to the predominant even Δj quantum propensity rule.

VI. SUMMARY AND CONCLUSION

Direct absolute state-to-state rate coefficients for RET in the CO-H_2 system at room temperature for

selected rotational levels j_i in the CO $X^1\Sigma^+$, $v = 2$ vibrational state were measured using time-resolved IR-VUV double resonance spectroscopy and compared to accurate 4-D quantum scattering calculations. The overall agreement is very good, enabling testing of the anisotropic part of the PES, which is critical for the robust high temperature quantum calculations needed to estimate rate coefficients which can be used to model the CO emission from, for example, photodissociation regions or protoplanetary disks.

Experimental evidence is reported for the first time for odd and even propensity rules for the CO-H_2 system. This represents a valuable and sensitive tool for benchmarking the anisotropy of the PES. This study also shows that the CO-H_2 system behaves in a significantly different way from the CO-He system from the perspective of both the magnitude and general trends of rate coefficients, including the propensity rules. These findings were made possible by the use of the time-resolved IR-VUV double resonance technique which is able to reveal quantum effects even in thermally averaged experiments thanks to high quantum-state selectivity. Finally, in future work, a more detailed theoretical investigation would be valuable (e.g. a partial-wave analysis), for a more comprehensive interpretation of the interference phenomenon in molecular scattering.

ACKNOWLEDGMENTS

We would like to thank David Carty, Laura Mertens and Martin Fournier for their assistance in the experiments. Thierry Stoecklin, Piotr Jankowski and Krzysztof Szalewicz are acknowledged for long-term collaboration and discussions on the theoretical aspects of this work. All the computations presented in this paper were performed using the GRICAD infrastructure (https://gricad.univ-grenoble-alpes.fr), which is supported by Grenoble research communities.
This work was supported by the Agence Nationale de la Recherche (ANR-HYDRIDES), contract ANR-12-BS05-0011-01, by the Région de Bretagne and the French National Programme "Physique et Chimie du Milieu Interstellaire" (PCMI) of CNRS/INSU with INC/INP cofunded by CEA and CNES.

[1] E. Roueff and F. Lique, Molecular Excitation in the Interstellar Medium: Recent Advances in Collisional, Radiative, and Chemical Processes, Chem. Rev **113**, 8906 (2013).
[2] A. Faure, Collisional rate coefficients for astrophysics, Proc Int Astron Union **18**, 123 (2022).
[3] S. Noll, B. Proxauf, W. Kausch, and S. Kimeswenger, Mechanisms for varying non-lte contributions to oh rotational temperatures from measurements and modelling. ii. kinetic model, J. Atmos. Sol.-Terr. Phys. **175**, 100 (2018).
[4] J. Voráč, P. Synek, V. Procházka, and T. Hoder, State-by-state emission spectra fitting for non-equilibrium plasmas: OH spectra of surface barrier discharge at argon/water interface, J. Phys. D: Appl. Phys. **50**, 294002 (2017).
[5] A. Jörg, U. Meier, R. Kienle, and K. Kohse-Höinghaus, State-specific rotational energy transfer in OH ($A^2\Sigma^+, v' = 0$) by some combustion-relevant collision partners, Appl. Phys. B **55**, 305 (1992).
[6] S. M. Jo, S. Venturi, J. G. Kim, and M. Panesi, Rovibrational internal energy transfer and dissociation of high-temperature oxygen mixture, J. Chem. Phys **158**, 064305 (2023).
[7] A. Ratanavis, N. Campbell, A. V. V. Nampoothiri, and W. Rudolph, Performance and Spectral Tuning of Optically Overtone Pumped Molecular Lasers, IEEE J. Quantum Electron **45**, 488 (2009).
[8] A. V. V. Nampoothiri, A. M. Jones, C. Fourcade-Dutin, C. Mao, N. Dadashzadeh, B. Baumgart, Y. Y. Wang, M. Alharbi, T. Bradley, N. Campbell, F. Benabid, B. R. Washburn, K. L. Corwin, and W. Rudolph, Hollow-core optical fiber gas lasers (HOFGLAS): a review, Opt. Mater. Express **2**, 948 (2012).
[9] W. Song, X. Zhang, Q. Zhang, Y. Hou, and P. Wang, 21.8 W acetylene-filled hollow-core anti-resonant fiber-amplified spontaneous emission source at 3.1 µm, Opt. Lett., OL **49**, 3636 (2024).
[10] J. Shi, X. Li, W. Pei, L. Lei, G. Lv, Z. Zhou, and Z. Wang, Mid-infrared pulsed fiber laser source at 4.3 μm based on a CO_2-filled anti-resonant hollow-core silica fiber, Opt. Express, OE **32**, 43033 (2024).
[11] R. B. Bernstein, Atom - molecule collision theory: A guide for the experimentalist, :Springer, New York(1979).
[12] H. Labiad, M. Fournier, L. A. Mertens, A. Faure, D. Carty, T. Stoecklin, P. Jankowski, K. Szalewicz, S. D. Le Picard, and I. R. Sims, Absolute measurements of state-to-state rotational energy transfer between CO and H_2 at interstellar temperatures, Phys. Rev., A **105**, L020802 (2022).
[13] S. Chefdeville, T. Stoecklin, A. Bergeat, K. M. Hickson, C. Naulin, and M. Costes, Appearance of Low Energy Resonances in CO-para-H_2 Inelastic Collisions, Phys. Rev. Lett **109**, 023201 (2012).
[14] B. Yang, P. Zhang, C. Qu, P. C. Stancil, J. M. Bowman, N. Balakrishnan, and R. C. Forrey, Inelastic vibrational dynamics of CS in collision with H2 using a full-dimensional potential energy surface, Physical Chemistry Chemical Physics (Incorporating Faraday Transactions) **20**, 28425 (2018).
[15] B. Yang, P. Zhang, C. Qu, P. C. Stancil, J. M. Bowman, N. Balakrishnan, and R. C. Forrey, Full-dimensional quantum dynamics of SO($X^3\Sigma^-$) in collision with H_2, Chemical Physics **532**, 110695 (2020).
[16] D. Hoffman, J. Taylor, T. J. Price, R. C. Forrey, B. H. Yang, P. C. Stancil, Z. E. Zhang, and N. Balakrishnan, Rovibrational Transitions in HCl due to Collisions with H_2: Spin-free and Hyperfine-resolved Transitions, Astro-

phys. J **969**, 7 (2024).

[17] A. Bergeat, J. Onvlee, C. Naulin, A. van der Avoird, and M. Costes, Quantum dynamical resonances in low-energy CO(j = 0) + He inelastic collisions, Nat. Chem **7**, 349 (2015).

[18] S. N. Vogels, T. Karman, J. Kłos, M. Besemer, J. Onvlee, A. van der Avoird, G. C. Groenenboom, and S. Y. T. van de Meerakker, Scattering resonances in bimolecular collisions between NO radicals and H_2 challenge the theoretical gold standard, Nature Chem **10**, 435 (2018).

[19] C. W. McCurdy and W. H. Miller, Interference effects in rotational state distributions: Propensity and inverse propensity, J. Chem. Phys **67**, 463 (1977).

[20] A. Faure, F. Lique, and L. Wiesenfeld, Collisional excitation of HC_3N by para- and ortho-H_2, MNRAS **460**, 2103 (2016).

[21] K. Imanzi, D. Bostan, M. McCrea, J. Featherstone, M. Brouard, and D. Babikov, Symmetry breaking: A classic example of quantum interference captured by mixed quantum/classical theory, J. Phys. Chem. Lett **14**, 10617 (2023).

[22] N. Bouhafs, C. Rist, F. Daniel, F. Dumouchel, F. Lique, L. Wiesenfeld, and A. Faure, Collisional excitation of NH_3 by atomic and molecular hydrogen, MNRAS **470**, 2204 (2017).

[23] N. Bouhafs, F. Lique, A. Faure, A. Bacmann, J. Li, and H. Guo, Rotational excitation of the interstellar NH_2 radical by H_2, J. Chem. Phys **146**, 064309 (2017).

[24] M. Lanza, Y. Kalugina, L. Wiesenfeld, and F. Lique, Near-resonant rotational energy transfer in HCl–H2 inelastic collisions, J. Chem. Phys **140**, 064316 (2014).

[25] C. Joblin, E. Bron, C. Pinto, P. Pilleri, F. Le Petit, M. Gerin, J. Le Bourlot, A. Fuente, O. Berne, J. R. Goicoechea, E. Habart, M. Köhler, D. Teyssier, Z. Nagy, J. Montillaud, C. Vastel, J. Cernicharo, M. Röllig, V. Ossenkopf-Okada, and E. A. Bergin, Structure of photodissociation fronts in star-forming regions revealed by Herschel observations of high-J CO emission lines, Astron. Astrophys. **615**, A129 (2018).

[26] P. Woitke, I. Kamp, and W.-F. Thi, Radiation thermochemical models of protoplanetary disks - I. Hydrostatic disk structure and inner rim, Astron. Astrophys **501**, 383 (2009).

[27] W. F. Thi, I. Kamp, P. Woitke, G. v. d. Plas, R. Bertelsen, and L. Wiesenfeld, Radiation thermo-chemical models of protoplanetary discs - IV. Modelling CO rovibrational emission from Herbig Ae discs, Astron. Astrophys **551**, A49 (2013).

[28] J. M. Hutson and S. Green, MOLSCAT: MOLecular SCATtering v. 14, Astrophysics Source Code Library, record ascl:1206.004 (2012).

[29] A. Faure, P. Jankowski, T. Stoecklin, and K. Szalewicz, On the importance of full-dimensionality in low-energy molecular scattering calculations, Sci. Rep. **6**, 28449 (2016).

[30] M. Stachowiak, E. Grabowska, X.-G. Wang, T. Carrington, K. Szalewicz, and P. Jankowski, Theory cracks old data: Rovibrational energy levels of $ortho H_2-CO$ derived from experiment, Science Advances **10**, eadj8632 (2024).

[31] P. Jankowski, Private communication.

[32] R. Hilbig and R. Wallenstein, Tunable VUV radiation generated by two-photon resonant frequency mixing in xenon, IEEE Journal of Quantum Electronics **19**, 194 (1983).

[33] L. A. Mertens, H. Labiad, O. Denis-Alpizar, M. Fournier, D. Carty, S. D. L. Picard, T. Stoecklin, and I. R. Sims, Rotational energy transfer in collisions between CO and Ar at temperatures from 293 to 30 K, Chem. Phys. Lett **683**, 521 (2017).

[34] D. Carty, A. Goddard, I. R. Sims, and I. W. M. Smith, Rotational energy transfer in collisions between $CO(X^1\Sigma^+, v = 2, J = 0, 1, 4$ and 6) and He at temperatures from 294 to 15 K, J. Chem. Phys. **121**, 4671 (2004).

[35] P. L. James, I. R. Sims, I. W. M. Smith, M. H. Alexander, and M. Yang, A combined experimental and theoretical study of rotational energy transfer in collisions between $NO(X^1\Pi_{1/2}, v = 3, J)$ and He, Ar and N_2 at temperatures down to 7 K, J. Chem. Phys. **109**, 3882 (1998).

[36] R. Englman and J. Jortner, The energy gap law for radiationless transitions in large molecules, Mol Phys **18**, 145 (1970).

[37] A. V. Smith and A. Wayne Johnson, Rotational transfer rates and propensity rule in nitric oxide-rare gas collisions, Chem. Phys. Lett **93**, 608 (1982).

[38] A. Gijsbertsen, H. Linnartz, C. A. Taatjes, and S. Stolte, Quantum interference as the source of steric asymmetry and parity propensity rules in NO – rare gas inelastic scattering, Journal of the American Chemical Society **128**, 8777 (2006).

[39] N. Furio, A. Ali, and P. J. Dagdigian, State-resolved study of collisional energy transfer between A $^2\Pi$ $v = 7$ and X $^2\Sigma^+$ $v = 11$ rotational levels of CN, J. Chem. Phys **85**, 3860 (1986).

[40] S. Antonova, K. Urbanski, A. M. Lyyra, F. C. Spano, and L. Li, State to state collision energy transfer in singlet states of Li_2, Chem. Phys. Lett **267**, 158 (1997).

[41] S. Antonova, A. Lin, A. P. Tsakotellis, and G. C. McBane, State to state He–CO rotationally inelastic scattering, J. Chem. Phys **110**, 2384 (1999).

[42] M. Mengel, F. C. De Lucia, and E. Herbst, Rate coefficients for rotationally inelastic collisions of CO with H_2, Canadian Journal of Physics **79**, 589 (2001).

[43] P. Jankowski and K. Szalewicz, Ab initio potential energy surface and infrared spectra of H_2-CO and D_2-CO van der Waals complexes, J. Chem. Phys **108**, 3554 (1998).

[44] B. C. Shepler, B. H. Yang, T. J. Dhilip Kumar, P. C. Stancil, J. M. Bowman, N. Balakrishnan, P. Zhang, E. Bodo, and A. Dalgarno, Low energy H+CO scattering revisited. CO rotational excitation with new potential surfaces, Astron. Astrophys **475**, L15 (2007).

[45] N. Balakrishnan, M. Yan, and A. Dalgarno, Quantum-Mechanical Study of Rotational and Vibrational Transitions in CO Induced by H Atoms, Astrophys. J **568**, 443 (2002).

[46] L. Song, A. van der Avoird, and G. C. Groenenboom, Three-dimensional Ab Initio potential energy surface for H–CO (X^2A'), J. Phys. Chem. A **117**, 7571 (2013).